Computers and Electronics in Agriculture 212 (2023) 108084

Contents lists available at ScienceDirect

Computers and Electronics in Agriculture

journal homepage: www.elsevier.com/locate/compag

Electrical resistivity tomography (ERT) measurements during water flow in a date palm stem segment

Tarig Bukhary [a,*], Johan Alexander Huisman [a], Haoran Wang [a], Egon Zimmermann [b], Harry Vereecken [a], Naftali Lazarovitch [c]

[a] Agrosphere (IBG-3), Institute of Bio- and Geosciences, Forschungszentrum Jülich, 52425 Jülich, Germany
[b] Electronic Systems (ZEA-2), Central Institute of Engineering, Electronics and Analytics, Forschungszentrum Jülich, 52425 Jülich, Germany
[c] French Associates Institute for Agriculture and Biotechnology of Drylands, The Jacob Blaustein Institutes for Desert Research, Ben-Gurion University of the Negev, Midreshet Ben Gurion 8490000, Israel

ARTICLE INFO

Keywords:
ERT
Irrigation
Date palm
Sap flow
Stem segment

ABSTRACT

Commercial cultivation of date palms has high economic significance, particularly in arid and hyper-arid regions. Achieving commercially viable yield of dates amid water scarcity and enforced restrictions on water use requires optimising the amount and timing of irrigation. To that end, better understanding of the temporal dynamics of the water use of date palm is of great importance. Traditionally, this can be achieved through sap flow estimates obtained using heat dissipation probes. However, such measurements lack the ability to provide information on the spatial distribution of sap flow, which is important considering that date palms transport water in the entire stem cross-section. The aim of this study is to evaluate whether electrical resistivity tomography measurements have the potential to provide information on the spatial variability of flow in date palm stems. For this, flow was induced through a stem segment that was obtained from a felled date palm tree. ERT measurements were continuously obtained throughout a cycle of flow and no-flow periods. The results showed that the mean bulk electrical conductivity varied strongly due to changes in the flow conditions. In addition, it was found that the electrical conductivity of the outflow was much higher than that of the inflow, which indicates the release of stored salt from the stem segment. Analysis of the spatial distribution of the electrical conductivity suggested that flow mainly occurred in a limited part of the cross-sectional area of the stem. Overall, it was concluded that the ERT is a promising tool to investigate the spatial variability of water flow in date palm stems.

1. Introduction

Date palm (Phoenix dactylifera L.) is a widely cultivated crop in arid Mediterranean regions, where it has considerable economic importance. The global production of date as a crop increased from 1.8 million tonnes in 1961 to 8.5 million tonnes today, and the date production industry is valued at over 1.2 billion United States Dollars (Zaid, 2002 ; Zaid, 2010; FAOSAT, 2018). In Israel, the commercial cultivation of date palms in the hyper-arid Arava and Jordan valleys (from the Sea of Galilee, along the Jordan valley to the Red Sea) has grown substantially in the past two decades. The number of date palms has increased to 850,000 palm trees covering an area of 7,000 ha, which is triple the number of planted trees in the early 1990s. Date palms are widely known to be well adapted to the climatic conditions of arid regions. However, they require irrigation with significant water volumes to achieve commercially viable yields. The irrigation volume required to achieve commercial yield is estimated at 2,500 mm/yr (Tripler et al., 2011). The maintenance of a viable economic value of dates as a crop amid water scarcity and water use restrictions in hyper-arid regions thus requires careful consideration of irrigation scheduling both in terms of amount and timing (Tripler et al., 2011). Due to the significant surge in agricultural productivity, local land management policies adopted new irrigation strategies in which marginal water resources are being utilised to the fullest potential (Tal, 2016). These marginal water sources, such as effluent and naturally saline water, are also increasingly used for irrigating date palms (Wiesman, 2009; Tripler et al., 2011). Since date palms have a limited tolerance to salinity (Maas and Hoffman, 1977), excessive exposure to such water sources has significant effects on the growth, yield, and water consumption of date palms. In addition, the use of such water sources leads to salinization of the root zone (Tripler et al.,

* Corresponding author.
E-mail address: t.bukhary@fz-juelich.de (T. Bukhary).

https://doi.org/10.1016/j.compag.2023.108084
Received 13 February 2023; Received in revised form 30 May 2023; Accepted 18 July 2023
Available online 29 July 2023

2011). Further restrictions on irrigation water use can thus be expected in the future considering the increasingly expanding date palm orchards.

The maximisation of date yield requires the optimisation of irrigation scheduling with the aim of closely matching the evapotranspiration requirements of date palms (Sperlinget al., 2015). This requires a better understanding of the temporal dynamics of date palm water use. Date palm, as a monocot species, falls within the category of plants incapable of renewing its vascular bundles with secondary growth in the trunk (Zimmermann and Tomlinson, 1972). As such, the entire growth span of date palms is served by primary vascular bundles containing both phloem and xylem (Sperry, 1986). A ground parenchymatous tissue with large intercellular air spaces hosts these vascular bundles, which are embedded uniformly into the tissue (Parthasarathy and Klotz (1976)). Such a stem structure potentially allows water flow in the entire cross-sectional area of the stem to support transpiration. Some studies found that a considerable amount of water is present in all active vacuolated parenchyma cells, therefore suggesting a potential internal storage capacity for water (Evert, 2006).

Sap flow measurements have been widely used to improve understanding of the temporal dynamics of date palm water use (Sellami and Sifaoui, 2003; Sperling et al., 2012). Such sap flow estimates are obtained using heat dissipation sensors that consists of one heated probe at a constant power, and a non-heated probe that measures the reference temperature (Sperling et al., 2012). The work by Sellami and Sifaoui (2003) and Sperling et al. (2012) showed that heat dissipation sensors that have been adapted to date palms can measure the sap flow at different heights of the date palm stem when the sensor is made long enough to reach the inner core of the stem where stable and massive water flow can be observed. It has also been reported that sap fluxes to the canopy are enriched by the removal of water from parenchymatous tissue into xylem vessels (Sperling et al., 2012; Sperling, 2013). Furthermore, mature date palms are reportedly capable of storing up to 1 m^3 of water in their trunks, which can supply 25% of daily transpiration (Sperling et al., 2015), and can thus contribute critically to sustaining transpiration during summer days (Meinzer et al., 2003; Cermak et al., 2007; Scholz et al., 2007). Sperling et al. (2012) reported that transpiration of date palms growing in weighing lysimeters was highly correlated to sap flow estimates obtained with heat dissipation sensors mounted in the upper part of a tree. It has also been argued that daily internal water storage dynamics of stem segments can be quantitatively evaluated using sap flow measurements at different heights along the stem (Köcher et al., 2013). Some studies found that sap flow in date palms differed during the morning, afternoon, and throughout the night (Sellami and Sifaoui, 2003; Sperling et al., 2012). Additionally, sap flow estimates at the upper part of the date palm were found to be much higher at noon compared to the lower part, and relatively lower at night (Sellami and Sifaoui, 2003; Sperling et al., 2015). Nevertheless, the calculation of whole-tree water use from point-scale sap flow measurements is practically challenging, considering the heterogeneous xylem hydraulic conductivity and the resulting variability in sap flow in the palm trunk.

Electrical methods such as electrical resistivity tomography (ERT) have been used for imaging of the bulk electrical conductivity distribution inside objects through the use of current injections and potential measurements (Ramirez et al., 2000; Aw et al., 2014; Binley and Slater, 2020). ERT has been successfully used for monitoring water infiltration (Daily et al., 1992; Hinnell et al., 2010), studying root zone water dynamics of crops (Srayeddin and Doussan, 2009; Garre et al., 2011), and determining tree root distributions (Amato et al., 2008; Zenone et al., 2008). Several studies have also used electrical methods to characterise tree trunk structure (Al Hagrey, 2007), including the separation of sapwood from the heartwood (Bieker et al., 2010; Guyot et al., 2013; Wang et al., 2016), assessing the effect of temperature variation and dehydration on tree stems (Ganthaler et al., 2019), and detecting wood decay and infections (Bieker and Rust, 2010; Brazee and Wick, 2011).

Given that sap flow measurements have the potential to provide reasonable budgetary estimates of whole-tree water use if information on the spatial distribution of trunk internal water flow and storage would be available (Wullschleger et al., 1998; Sperling, 2013), the key idea of this study is to combine sap flow measurements with the non-invasive tomographic capabilities of ERT. In this context, the aim of this study is to explore whether electrical properties can be used as a proxy to monitor the flow and temporal dynamics of water in a stem segment of a date palm. This is realised by obtaining continuous ERT measurements while inducing flow in a stem segment under varying conditions during a flow experiment in a laboratory environment. Using this approach, this study further aims to establish a better understanding on the correlation between hydraulic and electrical properties of the stem wood, and to evaluate the potential of ERT measurements in monitoring the spatial variation in sap flow. In the following, the details of the flow experiment are described first. Then, the results of the continuous ERT and other relevant measurements are presented and discussed.

2. Materials and methods

2.1. Measurement Set-up

Fig. 1 shows a schematic illustration of the measurement set-up used in this study. A stem segment was obtained from a felled date palm (Phoenix dactylifera L. cv. Medjool) in Israel, which was then placed in a Polyethylene container and covered in epoxy to reduce microbiological activity and to allow for transportation to Germany. Upon arrival, the epoxy was removed and the segment was cleared from bark wood. Next, it was processed in a wood turning machine to a cylindrical shape with a diameter of 0.25 m and a length of 0.50 m. The outside of the sample was sealed with a liquid plastic coating (Plasti-Dip, Performix, Germany) in multiple layers. The coating layers were applied on the sample while slowly rotating horizontally in the wood turning machine, thus ensuring a constant thickness for the coating. Each layer applied was allowed to adequately dry for up to a day before the following layer was applied. The two ends (top and bottom) of the processed stem segment were exposed, and a plastic funnel was placed and fitted on the top end and sealed in place using self-expanding sealing foam (Benson et al., 2019). The stem segment was positioned in the same orientation as the felled date palm, thus maintaining the same organic flow direction from the bottom up. The stem segment was placed in a water-filled basin and elevated while ensuring that the exposed bottom end was submerged by at least 20 mm of water (Fig. 1). A reservoir containing the flow solution was connected to the basin by means of plastic tubing, and a peristatic pump (Concept 2105mcs, SAIER Verpackungstechnik GmbH, Alpirsbach, Germany) was used to deliver the solution at a constant rate. A vacuum pump (N820.3AN.18, Neuberger, Freiburg, Germany) was connected to the funnel at the top end (Fig. 1). Between the vacuum pump and the funnel, a container was used to collect the outflowing solution and a pressure gauge and a ceramic pin pressure regulator were used to control the applied suction (Fig. 1). The amounts of inflow and outflow (Q_{in} and Q_{out}, Fig. 1) were monitored by means of weighing using balances (MC1, Sartorius AG, Göttingen, Germany, accuracy $\pm$ 0.1 g). The electrical conductivity of the inflow and outflow solutions were measured using a handheld EC meter (WTW, Multi 3320).

Using this set-up, a flow experiment with three flow periods with vacuum pressures of −0.3, −0.2, and −0.1 bar was performed. It should be noted that these vacuum pressures were selected based on the ability of the used vacuum pump, and do not reflect realistic field conditions nor scenarios of water availability. For each flow period, the inflow solution was a 0.015 M KCl solution with an electrical conductivity of 0.04 S/m. Each flow period was followed by a no-flow period. The duration of each flow and no-flow period is presented in Table 1.

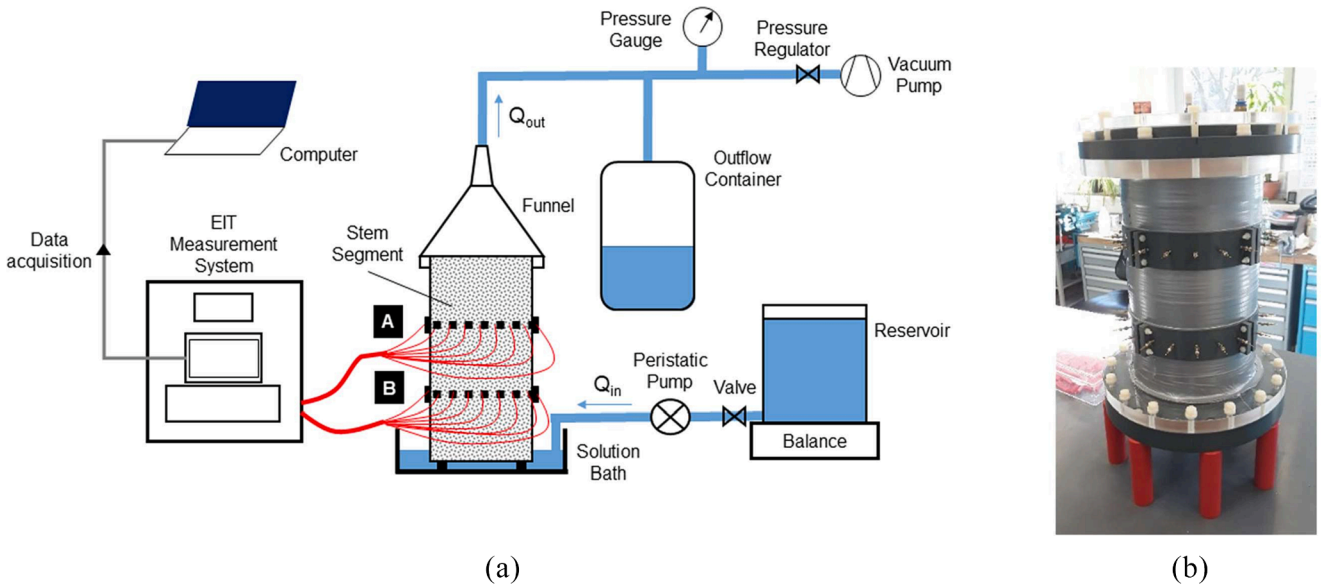

Fig. 1. *a)* A schematic illustration of the measurement set-up (the letters A and B refer to the upper and lower electrode layers, respectively); and *b)* a picture showing the stem segment at the end of the processing stage.

Table 1
Duration of flow and no-flow periods and the volumes of the solution introduced.

Designation	Duration [hr]	Vacuum Pressure Applied [bar]	Solution Volume Introduced [*l*]	Estimated Flow Rate [*l*/hr]
Flow Period I	8.81	− 0.3	10.63	72.36
No-Flow Period I	17.78	–	–	–
Flow Period II	7.75	− 0.2	4.77	36.91
No-Flow Period II	14.32	–	–	–
Flow Period III	8.69	− 0.1	0.50	3.45
No-Flow Period III	9.57	–	–	–

2.2. ERT system and data acquisition

To enable ERT measurements, two rings of 20 electrodes at heights of 0.167 and 0.333 m were used (Fig. 1). For this, brass electrodes were installed into the stem segment to a depth of 6 mm at equidistant positions. To ensure that the electrodes remained securely in place, two binding rings were used (Fig. 1b). The electrodes in the upper ring were numbered from 1 to 20, whereas the electrodes in the lower ring were numbered from 21 to 40. The electrodes of both rings were connected to the custom-made EIT40 system (Zimmermann et al., 2008) used for ERT measurements. This system measures the voltage relative to the system ground at all electrodes apart from the current injection pair. This allows to determine the potential differences between electrodes during post-processing. With this measurement approach, only the current injection electrode pairs need to be specified prior to the ERT measurements. It also allows for making consecutive measurements at high temporal resolution. The system design as well as correction methods for measurement errors are described in detail in Zimmermann et al. (2008) and Zimmermann (2010).

To monitor the flow experiment, ERT measurements were acquired independently for the two rings of electrodes. Current injection electrode pairs were specified in a circulating sequence, where 10 electrodes were skipped between the electrode pair used for current injection for every measurement (i.e. 1–12, 12–3, 3–14, … for the upper ring). This sequential acquisition was continued until the circulating scheme reached the initial electrode pair again (i.e., electrodes 10–1 for the last current injection). A skip-10 acquisition arrangement ensured that the current pairs were located across two different ends of the plane, thus avoiding superficial penetration of the current. This resulted in 20 current injections per ring, where each electrode was used an equal number of times for current injection. Each current injection consisted of three repeated measurements. Measurements were obtained alternately at the two electrode layers (A and B, Fig. 1) at a temporal resolution of 4.60 min using a current frequency of 164.3 Hz. The four-point measurements were then constructed in post-processing using a complete configuration strategy (Xu and Noel, 1993; Blome et al., 2011), which theoretically contains the complete information content. In particular, all pairs of electrodes used for current injection were also used as pairs for potential measurements, which are located on opposite sides of the stem segment (e.g. potential pairs 2–11, 2–13, … for a current injection at 1–12 for the upper ring). This protocol resulted in a total of 340 ERT measurements per electrode ring. Prior to inverting the data, measurements with an absolute geometric factor greater than three times the average were removed (40 measurements). The real part of the measured transfer impedances from repeated measurements were then averaged and used for data inversion.

2.3. ERT inversion

The data was inverted using a MATLAB-based customised programme developed by Zimmermann (2011) using a 3-D mesh generated using the finite element grid generator Gmsh (Geuzaine and Remacle, 2009). In particular, a Gauss-Newton algorithm was used to iteratively minimise the following objective function:

$$\Psi(m) = \Psi_d + \lambda\Psi_m = ||W_d[d - f(m)]||^2 + \lambda||W_m m||^2 \quad (1)$$

where Ψ_d and Ψ_m are the data misfit and model regularisation, respectively, W_d is the data weighting matrix, d is the measured transfer impedance, $f(m)$ is the modelled transfer impedance of model m, λ is the regularisation parameter, and W_m is the model roughness filter. The value of λ was obtained using an approximated L-curve approach (Li (1999); Günther, 2004). A limited range of potential λ values was evaluated by linearising the inversion. In particular, the Jacobian matrix calculated using the starting homogeneous model was used to update

the model parameter, and to approximate the forward response. The resulting data misfit $\psi_d(\lambda)$ was then plotted against the model regularisation $\psi_m(\lambda)$ in a log–log space, which forms an L-shaped curve. The optimum regularisation parameter λ was determined from the corner of the approximated L-curve using the maximum curvature method, where the corner is located at the point where the calculated curvature c of the parametric function ($\psi_d(\lambda)$, $\psi_m(\lambda)$) reaches a maximum (Hansen, 1992; Hansen and Oleary (1993); Günther, 2004). For a meaningful comparison of the imaging results within a time series, all datasets were inverted with the same λ value. A value of $\lambda = 1.25$ was selected after determining the optimum value for λ at key observation times during the flow experiment. Using this fixed λ, the data were inverted using equal weighting and six iterations of the Gauss-Newton algorithm, which ensured that convergence was reached.

3. Results and discussion

The development of the average real part of the electrical conductivity *Re(σ)* obtained from the ERT inversion results is presented in Fig. 2 for the upper and lower planes for the entire duration of the flow experiment. The dashed lines mark the start and end of each flow period, respectively. The average *Re(σ)* of both planes is higher than the electrical conductivity σ of the introduced solution (0.04 S/m) for the entire duration of the experiment. A clear difference can also be observed between the average *Re(σ)* of both planes, with the lower plane exhibiting higher values by 20% ~ 30 % than the upper plane (Fig. 2), which is interpreted as variation in the structure of the stem itself and not in terms of water flow. Fig. 3 shows the measured electrical conductivity of the in- and outflow for the three flow periods. It can be seen that the measured σ of the outflow is considerably higher than that of the introduced solution. It can also be observed that the measured σ of the outflow increased with declining vacuum pressure (Fig. 2) and the resulting lower flow rates, which is attributed to the longer contact time between the introduced solution and the stem segment. These results suggest the presence of stored salt within the stem segment that is being released into the outflow. These stored salts likely originated from irrigation water prior to the felling of the date palm. Fig. 2 also shows that differences in applied vacuum pressure resulted in different responses of the average *Re(σ)* for each flow period at both planes. The delay observed in the increase of the average *Re(σ)* during the third flow period is again attributed to the low flow rate associated with the lowest vacuum pressure applied (-0.1 bars).

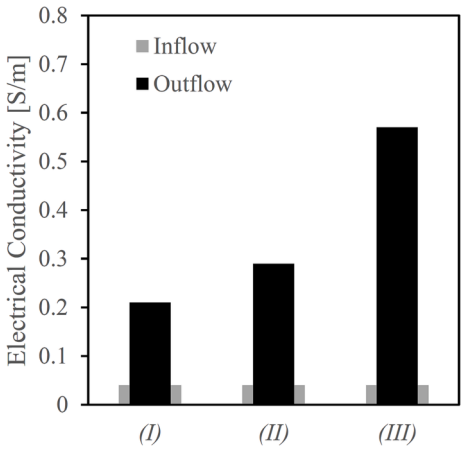

Fig. 3. Measured electrical conductivity of the inflow and outflow in S/m for the first, second, and third flow period (*I* through *III*), respectively.

The induced flow during each flow period resulted in an increase in the average *Re(σ)* at both planes. This increase occurred despite the use of an inflow solution with low measured σ, suggesting that it corresponds to a saturation process in the stem segment. A different temporal development for this on-going saturation process can be observed at the upper and lower planes. In the upper plane, electrical conductivity and thus saturation showed a gradual increase, whereas the lower plane showed a more rapid increase at the start of the flow. While the observed patterns are similar for the second and third flow periods, the first flow period appears to differ distinctly at the start with a higher starting value of *Re(σ)* compared to the remaining flow periods (10% and 25% of the measured σ during the first no flow period for the lower and upper planes, respectively). This is attributed to the condition at which the stem segment was prior to the start of the experiment. The stem segment was sealed the night after a test run before the actual experiment commenced and was not allowed to drain freely as opposed to the conditions prior to initiating the other two flow periods.

Fig. 4 shows the spatial distribution of *Re(σ)* at the two planes for selected points in time (Fig. 2) for the three flow periods, which are discussed first followed by the results for the no-flow periods. It is clear that *Re(σ)* shows a heterogeneous spatial distribution during each flow period at both planes. The variation in the spatial distribution of the

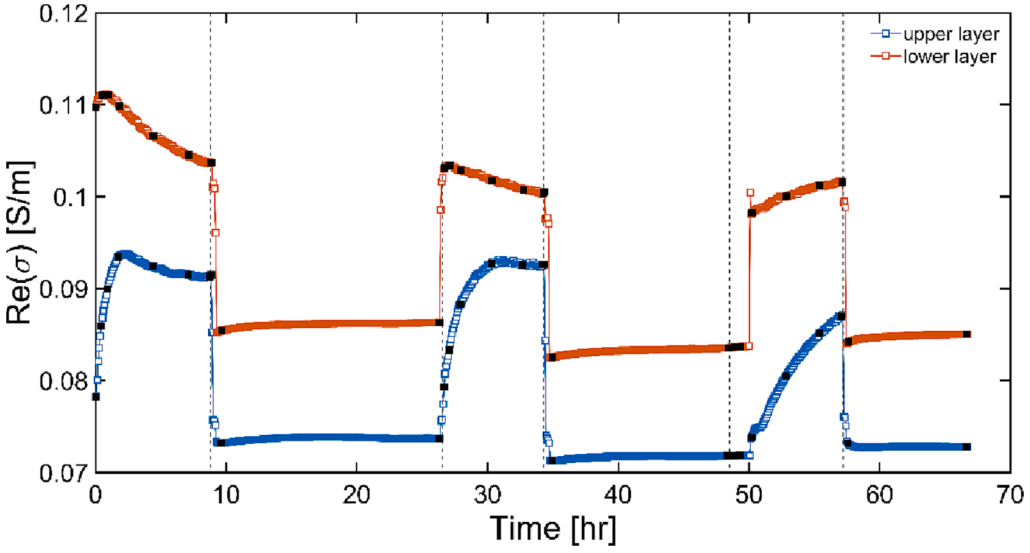

Fig. 2. Average bulk electrical conductivity in S/m of the two planes for the full duration of the flow experiment. The dashed lines mark the points in time when the vacuum pump was switched on and off. The black squares show selected points in time for each flow and no-flow period that are shown in Figs. 4 and 5.

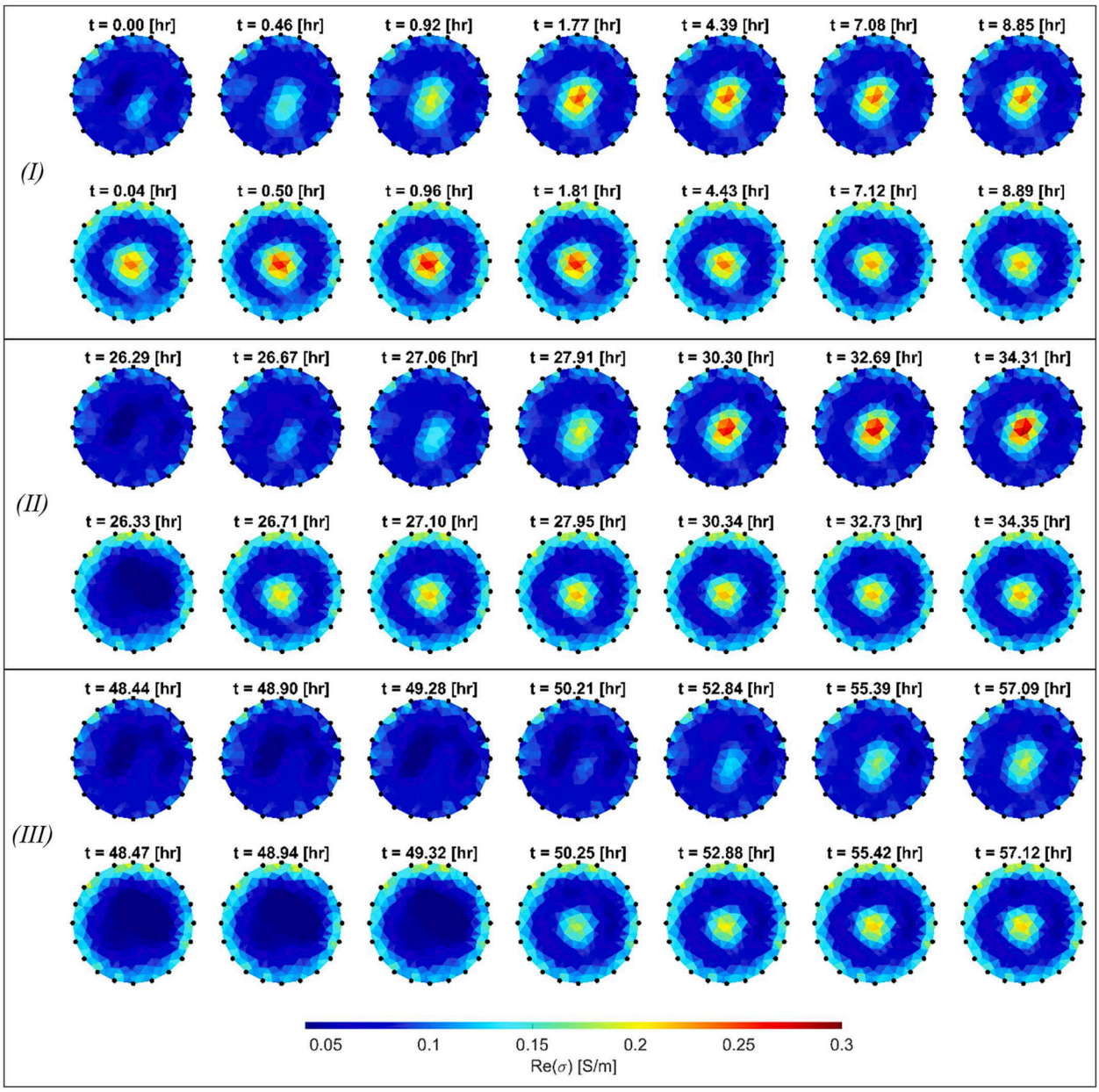

Fig. 4. Spatial distribution of the real part of the electrical conductivity *Re(σ)* in S/m for the three flow periods (*I* through *III*), for the upper (top rows per flow period) and lower (bottom rows) plane at selected points in time (in hours) as indicated in Fig. 2. Electrode positions are representated with black points.

electrical conductivity over the two planes is consistent throughout the three flow periods and involves a specific yet limited area in the centre of the two planes. This may be attributed to the limited number of vascular bundles (VB) of xylem vessels within the stem that are activated by the vacuum pressure applied, expectedly only those with a diameter that is small enough for the vacuum pressure applied to overcome capillary forces. The delay in the arrival of the introduced solution due to the reduction in the vacuum pressure can also be clearly observed in the spatial distribution of the electrical conductivity.

After removing the applied vacuum pressure, a sharp decrease in the average *Re(σ)* can be observed at both planes (Fig. 2), with a 22% decrease at the upper plane and a 25% decrease at the lower plane, which indicates the presence of a drainage process. It is evident that the expected saturation and drainage of the sample happen quickly. The increase in the average *Re(σ)* following the initiation of the flow is observed early on during each flow period. The drainage process appears to take place nearly instantaneously with the switching off of the pump, as shown by the sharp drop in the value of the averaged *Re(σ)* (Fig. 2). A closer look at the timing of the increase (saturation) and decrease (drainage) in the averaged *Re(σ)* at both planes shows the expected lag in the response observed in the upper plane compared to the lower plane (Fig. 2). Apart from the starting point at the beginning of the measurement period for both planes (Fig. 2), the averaged *Re(σ)* in the no-flow periods exhibits similar levels.

The observed consistency in variation of the spatial distribution of the electrical conductivity of the two planes during the flow periods becomes more apparent when observing the spatial distribution during the no-flow periods, which is presented in Fig. 5 for selected points in time (Fig. 2). As already discussed above, the drop in the *Re(σ)* and the advancement of the drainage process happen quickly following the switching off of the vacuum pump. After drainage, the spatial distribution of *Re(σ)* shows little variability in the centre of the stem segment throughout the no-flow period. These results suggest that only a limited area of the two planes is involved in contributing to the flow.

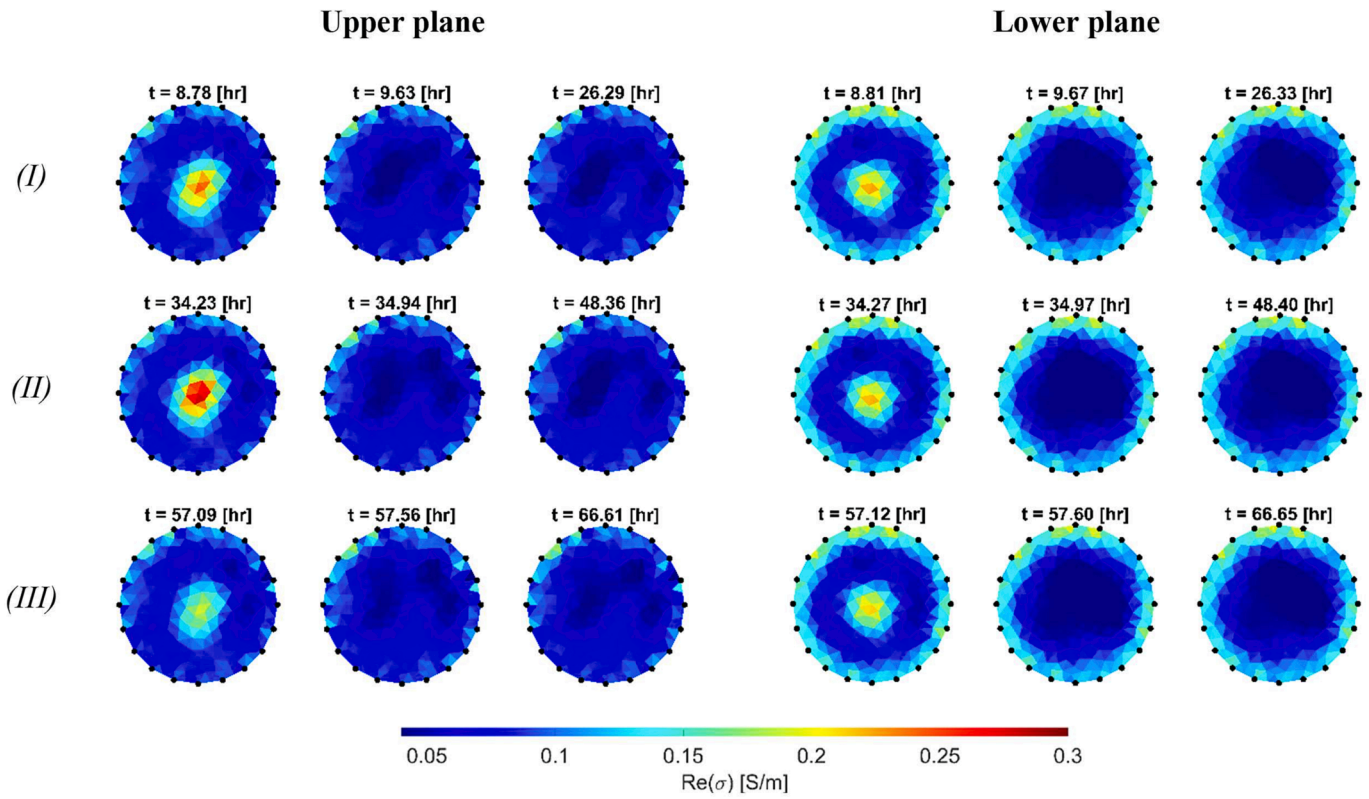

Fig. 5. Spatial distribution of the real part of the electrical conductivity *Re(σ)* in S/m for selected points in time (in hours) as indicated in Fig. 2 for the three consecutive no-flow periods (*I*, *II*, and *III*), respectively. The first column of each section (first from left, *I* through *III*) indicates the last point during the flow period (the moment of pump switching off). Electrode positions are marked with black points.

To further highlight the spatial heterogeneity in *Re(σ)*, the temporal development of *Re(σ)* at three selected positions per plane is shown in Fig. 6. The strongest dynamics in *Re(σ)* can be observed at the position closest to the centre of both planes. The dynamics become less apparent the further away the selected position is from the centre. The variation in *Re(σ)* is nearly negligible at the position that is furthest away from the centre (P2, Fig. 6) when compared to that closest to the centre (P3, Fig. 6), more so in case of the lower plane than the upper plane. This inspires confidence that the selected strategy to analyse time-lapse ERT measurements provides robust and temporally consistent inversion results. The presented time series at selected locations further emphasise that only a limited area per plane is involved in the flow. It is worth noting that the strong variation of *Re(σ)* at the position closest to the centre of each plane resembles that of the averaged *Re(σ)* for both planes (Fig. 2). In addition, this analysis shows that it is the change in electrical conductivity relative to the background that indicates flow, which is therefore analysed in more detail next.

Fig. 7 shows the relative difference to a reference measurement for selected points in time (Fig. 2). The reference time was selected as the corresponding measurements at times t = 16.69 hr and t = 16.73 hr for the upper and lower planes, respectively. This reference point falls within the first no-flow period (Fig. 2) and is considered more suitable as a datum for comparison than the start of the experiment due to the previously noted deviating initial conditions. For the upper plane, the change in *Re(σ)* is mainly observed as a steady increase during each flow period (prominently at the centre), that is proportional to the vacuum pressure applied, followed by a decrease during the no-flow periods. The same can be observed at the lower plane, although both the increase and the decrease in *Re(σ)* are larger compared to the upper plane. The breakthrough of the solution is observed sooner at the lower plane, which is in agreement with what is expected given the position of each plane relative to the flow direction. As previously observed, the centre of both planes appears to exhibit most of changes happening during and between flow and no-flow periods, and the difference in *Re(σ)* between the upper and lower layers remains consistent throughout the three no-flow periods.

4. Conclusions and outlook

In this study, continuous ERT measurements with high temporal resolution allowed to determine the spatial distribution of flow in a stem segment of a date palm. The electrical conductivity of the collected outflow from the stem segment was much higher than that of the inflow, thus suggesting the presence of stored salt in the stem segment that was released with the water flow. The development and the spatial distribution of the electrical conductivity at the two electrode layers differed with the applied vacuum pressure, which was clearly seen in the times at which changes were observed in the electrical conductivity at both planes. Overall, the results suggest a quick response in the electrical conductivity to the solution introduced at varying vacuum pressures, which makes measuring at high temporal resolution desirable. The results also show that the stem segment has undergone no drastic changes following each induced flow as observed during each no-flow period, despite the variation in applied vacuum pressure and the resulting differences in flow velocity in the stem segment. Following a brief period of rapid drainage, the stem segment remained at a stable state until the start of the next flow period. Although response time differed with the applied vacuum pressure, the area within each plane that showed the strongest dynamics in electrical conductivity was found to be rather similar in all flow periods, suggesting that a limited area per plane contributed to the flow in the stem segment.

Measuring with a high temporal resolution proved useful in capturing key developments in the electrical conductivity at the two planes, which provides confidence in the suitability of such

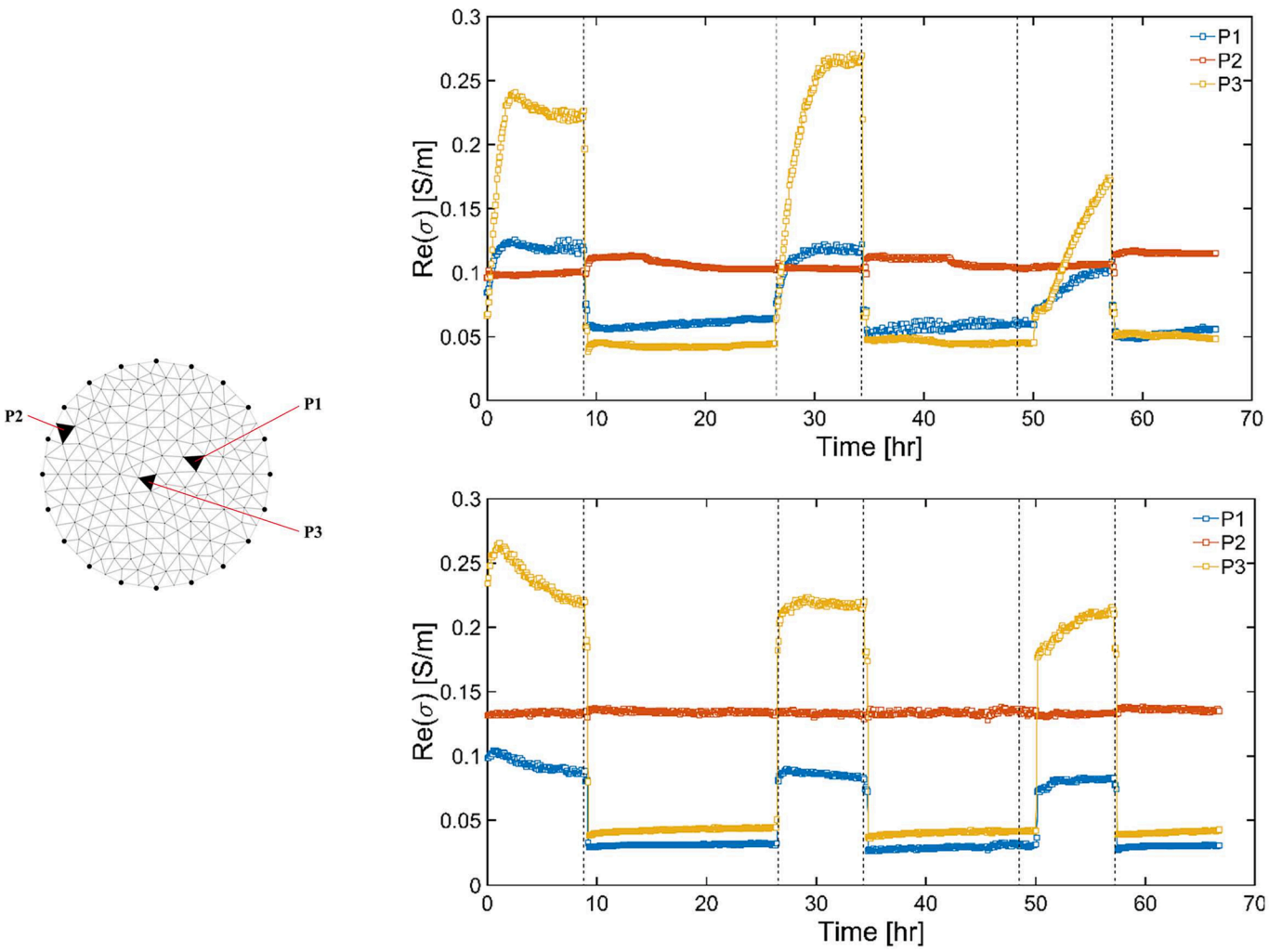

Fig. 6. Real part of the electrical conductivity in S/m throughout the duration of the experiment for the upper (top right) and lower (bottom right) planes at three selected positions (left). The dashed lines mark the start and end of each flow period, while electrode positions are marked with black points.

measurement for meaningful monitoring of water flow and storage in living trees. Overall, the results suggest that electrical measurements can be used to support the determination of sap flow and water storage within the trunk of living date palms. For example, it would be of great interest to make ERT measurements before installing sap flow sensors, as acquiring an idea of the most active area of the stem would potentially optimise not only the estimation of the sap flux density (by estimating the cross-sectional area of stem that is involved in the flow), but also the selection of the observation point where the sensor probe is installed in the trunk. This does not only apply to date palm trees, but is just as relevant for dicot tree species where the area of sapwood typically also needs to be known to upscale sap flow measurements to the scale of the tree.

To investigate diurnal changes in water storage and sap flow, a similar measurement set-up to what was used in this study can be employed. For example, ERT measurements could be made at two heights: at the lower trunk (e.g. at 1.0 m height from the ground) and in close proximity to the crown leaves. Using a similar acquisition strategy to what was employed in this study, the spatial distribution of the electrical conductivity at each electrode layer can be determined with a high temporal resolution. Based on the imaging results, heat dissipation probes can be installed at different depths in the stem at the height of the electrode rings to explore relationships between changes in electrical conductivity and sap flow estimates from the different probes installed. By measuring continuously for a fixed period of time, a baseline can be established for the electrical conductivity distribution during high and low transpiration periods during the diurnal cycle. Areas of high water flow within the stem can then be identified from their correlation to high electrical conductivity. Furthermore, subjecting the date palm to stress by suspending irrigation for a number of days would expectedly propagate in the electrical conductivity distribution at each plane, notably with a decrease in the areas exhibiting high electrical conductivity. These aspects will be investigated in a follow-up study using ERT measurements and sap flow measurements installed in juvenile date palms growing in lysimeters and mature date palms in an orchard.

Funding

This work was completed as part of a project entitled Integrating Electrical Resistivity Tomography and sap flow measurements within agro-ecosystem models to improve irrigation efficiency of date palm (PALM-IRRI), a joint cooperation between Forschungszentrum Jülich GmbH, and Ben-Gurion University of the Negev within the framework of the Joint German-Israeli Water Technology Research Programme. It was funded by the German Federal Ministry of Education and Research (BMBF) – Funding code: 02WIL1524; and the Ministry of Innovation, Science and Technology of the State of Israel – Funding code: 8769712.

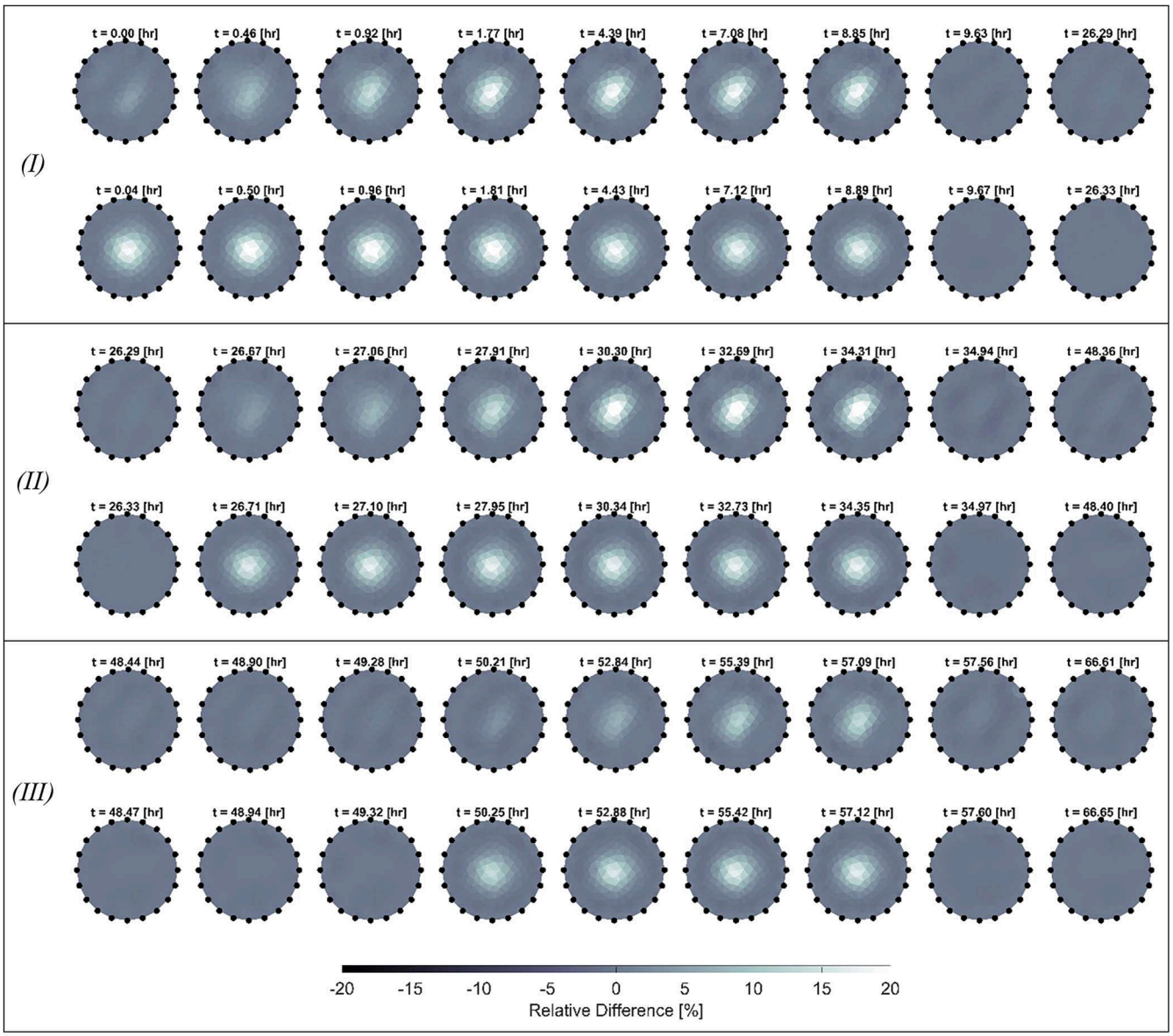

Fig. 7. Relative difference in the real part of the electrical conductivity $Re(\sigma)$ as a percentage to the measurement point at t = 16.69 hr and 16.73 hr for upper and lower planes, respectively at selected key points in time (in hours) as indicated in Fig. 2 throughout the full duration of the measurement presented for one consecutive flow and no-flow period (*I*, *II*, and *III*), respectively per plane (upper panels for upper layer and lower panels for lower plane). Electrode positions are marked with black points.

Declaration of Competing Interest

The authors declare the following financial interests/personal relationships which may be considered as potential competing interests: [Tarig Bukhary reports financial support was provided by the German Federal Ministry of Education and Research (BMBF). Tarig Bukhary reports financial support was provided by the Ministry of Innovation, Science and Technology of the State of Israel].

Data availability

Data will be made available on request.

Acknowledgements

The authors would like to extend their gratitude to Franz-Hubert Haegel and Odilia Esser for their valuable contribution and assistance in the planning, setting up, and implementation of the experiment.

References

Al Hagrey, S.A., 2007. Geophysical imaging of root-zone, trunk, and moisture heterogeneity. J. Exp. Bot. 58 (4), 839–854.
Amato, M., Basso, B., Celano, G., Bitella, G., Morelli, G., Rossi, R., 2008. In situ detection of tree root distribution and biomass by multi-electrode resistivity imaging. Tree Physiol. 28 (10), 1441–1448.
Aw, S.R., Rahim, R.A., Rahiman, M.H.F., Yunus, F.R.M., Goh, C.L., 2014. Electrical resistance tomography: A review of the application of conducting vessel walls. Powder Technol. 254, 256–264.
Benson, A.R., Koeser, A.K., Morgenroth, J., 2019. Estimating conductive sapwood area in diffuse and ring porous trees with electronic resistance tomography. Tree Physiol. 39 (3), 484–494.
Bieker, D., Rust, S., 2010. Non-destructive estimation of sapwood and heartwood width in scots pine (Pinus sylvestris L.). Silva Fennica 44 (2), 267–273.
Bieker, D., Kehr, R., Weber, G., Rust, S., 2010. Non-destructive monitoring of early stages of white rot by Trametes versicolor in Fraxinus excelsior. Ann. For. Sci. 67 (2), 7.
Binley, A., Slater, L., 2020. Resistivity and Induced Polarization: Theory and Applications to the Near-Surface Earth. Cambridge University Press, Cambridge.
Blome, M., Maurer, H., Greenhalgh, S., 2011. Geoelectric experimental design – Efficient acquisition and exploitation of complete pole-bipole data sets. Geophysics 76 (1), F15–F26.

Brazee, N.J., Wick, R.L., 2011. Armillaria species distribution and site relationships in Pinus- and Tsuga-dominated forests in massachusetts. Can. J. For. Res. 41 (7), 1477–1490.
Cermak, J., Kucera, J., Bauerle, W.L., Phillips, N., Hinckley, T.M., 2007. Tree water storage and its diurnal dynamics related to sap flow and changes in stem volume in old-growth Douglas-fir trees. Tree Physiol. 27 (2), 181–198.
Daily, W., Ramirez, A., Labrecque, D., Nitao, J., 1992. Electrical-resistivity tomography of vadose water-movement. Water Resour. Res. 28 (5), 1429–1442.
Evert, R.F., 2006. Esau's Plant Anatomy: Meristems, Cells, and Tissues of the Plant Body: Their Structure, Function, and Development, (3 ed.): John Wiley & Sons Inc.
FAOSAT (2018). Food and Agricultural Organisation of the United Nations http://www.fao.org/faostat.
Ganthaler, A., Sailer, J., Bar, A., Losso, A., Mayr, S., 2019. Noninvasive analysis of tree stems by electrical resistivity tomography: Unraveling the Effects of temperature, water status, and electrode installation. Front. Plant Sci. 10, 12.
Garre, S., Javaux, M., Vanderborght, J., Pages, L., Vereecken, H., 2011. Three-dimensional electrical resistivity tomography to monitor root zone water dynamics. Vadose Zone J. 10 (1), 412–424.
Geuzaine, C., Remacle, J.F., 2009. Gmsh: A 3-D finite element mesh generator with built-in pre- and post-processing facilities. Int. J. Numer. Meth. Eng. 79 (11), 1309–1331.
Günther, T. (2004). Inversion Methods and Resolution Analysis for the 2D / 3D Reconstruction of Resistivity Structures from DC Measurements. (Doctoral Thesis). Freiberg University of Mining and Technology.
Guyot, A., Ostergaard, K.T., Lenkopane, M., Fan, J.L., Lockington, D.A., 2013. Using electrical resistivity tomography to differentiate sapwood from heartwood: Application to conifers. Tree Physiol. 33 (2), 187–194.
Hansen, P.C., 1992. Analysis of discrete ill-posed problems by means of the l-curVE. SIAM Rev. 34 (4), 561–580.
Hansen, P.C., Oleary, D.P., 1993. The use of the l-curve in the regularization of discrete III-Posed Problems. SIAM J. Sci. Comput. 14 (6), 1487–1503.
Hinnell, A.C., Ferre, T.P.A., Vrugt, J.A., Huisman, J.A., Moysey, S., Rings, J., Kowalsky, M.B., 2010. Improved extraction of hydrologic information from geophysical data through coupled hydrogeophysical inversion. Water Resour. Res. 46, 14.
Köcher, P., Horna, V., Leuschner, C., 2013. Stem water storage in five coexisting temperate broad-leaved tree species: Significance, temporal dynamics and dependence on tree functional traits. Tree Physiol. 33 (8), 817–832.
Li, Y., & Oldenburg, D. (1999). 3-D Inversion of DC Resistivity Data Using an L-curve Criterion. Seg Technical Program Expanded Abstracts.
Maas, E.V., Hoffman, G.J., 1977. Crop salt tolerance—Current assessment. J. Irrig. Drain. Div. 103 (2), 115–134.
Meinzer, F.C., James, S.A., Goldstein, G., Woodruff, D., 2003. Whole-tree water transport scales with sapwood capacitance in tropical forest canopy trees. Plant Cell Environ. 26 (7), 1147–1155.
Parthasarathy, M.V., Klotz, L.H., 1976. PALM wood.1. Anatomical aspects. Wood Sci. Technol. 10 (3), 215–229.
Ramirez, A., Daily, W., Binley, A., 2000. Electrical resistance tomography. Lead. Edge 23.
Scholz, F.G., Bucci, S.J., Goldstein, G., Meinzer, F.C., Franco, A.C., Miralles-Wilhelm, F., 2007. Biophysical properties and functional significance of stem water storage tissues in Neotropical savanna trees. Plant Cell Environ. 30 (2), 236–248.
Sellami, M.H., Sifaoui, M.S., 2003. Estimating transpiration in an intercropping system: Measuring sap flow inside the oasis. Agric Water Manag 59 (3), 191–204.
Sperling, O., 2013. Water Relations in Date Palm Trees – a Combined Approach using Water, Plant, and Atmospheric Data. Ben Gurion University of the Negev (Doctoral Thesis).
Sperling, O., Shapira, O., Cohen, S., Tripler, E., Schwartz, A., Lazarovitch, N., 2012. Estimating sap flux densities in date palm trees using the heat dissipation method and weighing lysimeters. Tree Physiol. 32 (9), 1171–1178.
Sperling, O., Shapira, O., Schwartz, A., Lazarovitch, N., 2015. Direct in vivo evidence of immense stem water exploitation in irrigated date palms. J. Exp. Bot. 66 (1), 333–338.
Sperry, J.S., 1986. Relationship of xylem embolism to xylem pressure potential, stomatal closure, and shoot morphology in the palm rhapis-excelsa. Plant Physiol. 80 (1), 110–116.
Srayeddin, I., Doussan, C., 2009. Estimation of the spatial variability of root water uptake of maize and sorghum at the field scale by electrical resistivity tomography. Plant and Soil 319 (1–2), 185–207.
Tal, A., 2016. Rethinking the sustainability of Israel's irrigation practices in the Drylands. Water Res. 90, 387–394.
Tripler, E., Shani, U., Mualem, Y., Ben-Gal, A., 2011. Long-term growth, water consumption and yield of date palm as a function of salinity. Agric Water Manag 99 (1), 128–134.
Wang, H.L., Guan, H.D., Guyot, A., Simmons, C.T., Lockington, D.A., 2016. Quantifying sapwood width for three Australian native species using electrical resistivity tomography. Ecohydrology 9 (1), 83–92.
Wiesman, Z. (2009). Key characteristics of the desert environment. In Desert Olive Oil Cultivation: Advanced Biotechnologies (pp. 31-53). San Diego: Elsevier Academic Press Inc.
Wullschleger, S.D., Meinzer, F.C., Vertessy, R.A., 1998. A review of whole-plant water use studies in trees. Tree Physiol. 18 (8–9), 499–512.
Xu, B.W., Noel, M., 1993. On the completeness of data sets with multielectrode systems for electrical-resistivity survey. Geophys. Prospect. 41 (6), 791–801.
Zaid, A., 2002. Date Palm Cultivation. Food and Agricultural Organisation of the United Nations.
Zaid, A. (2010). The World Date Production: A Challenging Case Study. Paper presented at the Date Palm Research and Development Programme. United Nations Office for Project Services/UNOPS.
Zenone, T., Morelli, G., Teobaldelli, M., Fischanger, F., Matteucci, M., Sordini, M., Armani, A., Ferre, C., Chiti, T., Seufert, G., 2008. Preliminary use of ground-penetrating radar and electrical resistivity tomography to study tree roots in pine forests and poplar plantations. Funct. Plant Biol. 35 (9–10), 1047–1058.
Zimmermann, E., 2011. Phasengenaue Impedanzspektroskopie und -tomographie für geophysikalische Anwendungen. Rheinischen Friedrich-Wilhelms-Universität Bonn (Doctoral Thesis).
Zimmermann, E., Kemna, A., Berwix, J., Glaas, W., Vereecken, H., 2008. EIT measurement system with high phase accuracy for the imaging of spectral induced polarization properties of soils and sediments. Meas. Sci. Technol. 19 (9), 9.
Zimmermann, M.H., Tomlinson, P.B., 1972. The Vascular System of Monocotyledonous Stems. Bot. Gaz. 133 (2), 141–155.
Zimmermann, E., Huisman, J., Kemna, A., Berwix, J., Glaas, W., Meier, H., Walters, B., Esser, O. (2010). Advanced electrical impedance tomography system with high phase accuracy. Paper presented at the 6th World Congress in Industrial Process Tomography.